How do Cyclopropane Fatty Acids Protect the Cell Membrane of Escherichia coli in Cold Shock?

Archita Maiti, Abhay Kumar, Snehasis Daschakraborty[*]

Department of Chemistry, Indian Institute of Technology Patna, Bihar 801106, India.

AUTHOR INFORMATION

Corresponding Author

[*]snehasis@iitp.ac.in

ABSTRACT

The cyclopropanation of unsaturated lipid acyl chains of some bacterial cell membranes is an important survival strategy to protect the same against drastic cooling. To elucidate the role of cyclopropane ring containing lipids, we have simulated the lipid membrane of Escherichia coli (E. coli) and two modified membranes by replacing the cyclopropane rings with either single or double bonds at widely different temperatures. It has been observed that the cyclopropane rings provide more rigid kinks in the lipid acyl chain compared to the double bonds and therefore further reduce the packing density of the membrane and subsequently enhance the membrane fluidity at low temperatures. They also inhibit the close packing of other lipids and deleterious phase separation by strongly interacting with them. Therefore, this study has explained why E. coli bacterial strain, susceptible to freezing environment, relies on the cyclopropanation of an unsaturated chain.

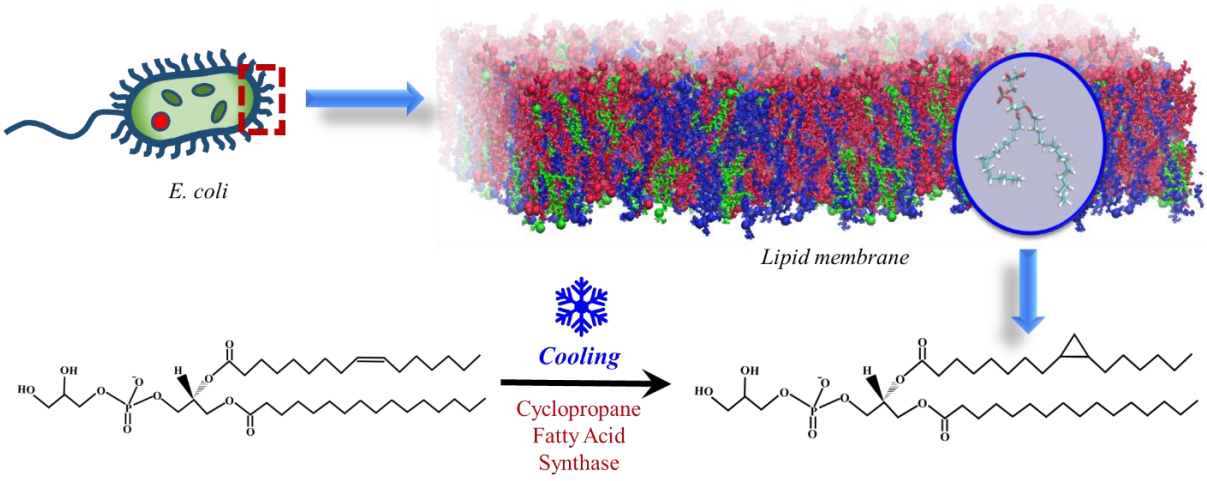

TOC Graphic

1. INTRODUCTION

Microorganisms often encounter various extreme challenges of the environment, which trigger continual adaptations of the cell membrane[1-2]. Under physiological condition, cell membrane is fluidic, which is necessary for performing its role in different cell biological processes. Drastic reduction of temperature is detrimental to the cell membrane since it may cause fluid-to-gel phase transition of the lipid bilayer[3-6] . In response to the environmental stress factors, the microorganisms have developed some key strategies, such as lipid remodelling homeoviscous adaptation[7-19], introducing small polar organic molecules (osmolytes)[3, 20-28] , etc. Lipids with unsaturated fatty acids (LUFAs) having kink in aliphatic chain introduces packing defects in the bilayer of lipids with saturated fatty acids (LSFAs) and thereby retain the membrane fluidity at lower temperature.

Another less common strategy for some specific microorganisms is cyclopropanation of the lipid acyl chains that protect the membrane from adverse effects of freezing during drastic cooling[29-34]. Lipids with cyclopropane ring containing fatty acids (LCFA) are widely distributed in a variety of organisms, particularly in bacteria, e.g., Escherichia coli, Lactobacillus, Rhizobium,[32] etc. They are generated in situ via methylation of the cis-unsaturated fatty acid double bond in presence of cyclopropane fatty acid synthase and the concentration of LCFAs rises as the cell is exposed to a hostile condition[29, 31-37]. LCFAs are known to disrupt the ordering of the lipid acyl chains and thereby keep the membrane fluid at lower temperatures[38,1, 31]. Similar effect of LUFA is already known[7-19] . Henceforth, the role of cyclopropane ring is akin with that of the double bond, as evident from the earlier literature survey.

So, what is the specific purpose of the cyclopropanation of an unsaturated lipid acyl chain? From the chemical reactivity perspective, it is known that double bonds are more

susceptible to oxidation and ozonolysis than the cyclopropane rings and thus the LCFAs are more stable compared to LUFA[31-32] . Beside the chemical stability, there might be some roles of LCFAs to protect the cell membrane from drastic physical change, which is detrimental for the functional behaviours of the cell membrane. The earlier work by Poger et al. compared the role of cyclopropane ring and C=C unsaturated bond on the fluidity and ordering of the lipid membrane[31] . They proposed, the LCFAs enhance the membrane fluidity by influencing the lipid packing and increasing the gauche defect formation. It was claimed that the effect is partly due to steric hindrance originated by the methylene bridge. Although the above study provided important insights about the role of the cyclopropane rings in maintaining the packing density and fluidity of a single component lipid membrane, the actual role is far from understood in real cell membrane of the bacteria, such as E. coli, Lactobacillus, etc., where tens of different types of lipids are present[16, 29, 39-40] and in inhospitable situation, like at low temperature when the membrane exists in gel phase. Therefore, it is important to understand how LCFAs stabilize a realistic cell membrane which is exposed to a drastic change of temperature.

For understanding the role of LCFAs in maintaining the fluidity of a realistic cell membrane under drastic cooling, we have simulated a model lipid membrane of E. coli bacteria[40] consisting of 14 different types of lipids from all-atom (AA) and coarse-grained (CG) resolution. To elucidate specific advantages of LCFAs, we have also simulated two additional membranes with modified lipidome by replacing all the cyclopropane rings with either C-C single bond or C=C double bonds. The fully hydrated membranes are simulated at 6 different temperatures: 250, 270, 290, 310, 330, and 350 K.

2. SIMULATION METHODOLOGY

2.1. Composition of the membrane

The fourteen-component realistic E. coli bacterial membrane is taken from literature[40] both for CG and AA-simulations. To examine the role of cyclopropane rings (CP) in the acyl chain of lipid over single or double bonds, we have prepared additional two modified membrane systems. The model E. coli membrane containing cyclopropane rings is denoted as NM (Native Membrane), in another system we have replaced all the cyclopropane rings with C-C single bonds and named it as MMS (Modified Membrane with Saturated chains), and in the third system we have replaced all the cyclopropane rings with C=C double bond and named it as MMU (Modified Membrane with Unsaturated chains). The naming of the lipids is done based on acyl chains followed by headgroup (Figure S1 of the Supporting Information (SI)). The double bonds or cyclopropane moieties are located between carbon 9 and 10 for the 16-carbon tails and between carbon 11 and 12 for the 18-carbon tails. Only cis- geometry is considered for the double bonds and cyclopropane rings as per the realistic E. coli membrane. Three types of lipids are present in membrane systems depending on the headgroup: cardiolipin (CL), phosphatidylglycerol (PG), phosphatidylethanolamine (PE). PE- and CL-lipids are charged lipids. Each CL- and PE-lipids contribute -2 and -1 respectively. Required number of monovalent Na ions are added for charge balance of the system. PE-lipids are present in highest proportion in all the membrane systems (about 73%), PG-lipids exist in intermediate quantity (22%), and, cardiolipins are present in least amount (only 5%). Based on saturation level in acyl chains, total five types of lipids are there: cyclopropane ring containing lipids (cyp.), fully saturated lipids (sat.), monounsaturated lipids (monounsat.), diunsaturated lipids (diunsat.), and triunsaturated lipids (triunsat.). NM system holds cyp., monounsat., and diunsat. lipids; MMS system contains sat., monounsat., and diunsat. lipids; MMU system comprises monounsat.,

diunsat., and triunsat. lipids. Lipid names, numbers, abundance, and presence of CP/unsaturations are listed in Table S1. The structure of the lipids both in all-atom (AA) and coarse grained (CG) resolution are shown in Table S2.

2.2 Modelling of the membrane

***Coarse-grained modelling*:** MD-simulations of the multicomponent membrane systems in AA-resolution is quite challenging because although it reproduces many of the structural properties of the membrane systems, it fails to reproduce the phase behaviour[41-45] . The major reasons are long simulation time for the mutual diffusion of various constituents (around microsecond ranges) and requirement of a larger system to exactly predict the phase behaviour of a multicomponent bilayer. But due to limited computational performance it is quite impossible to perform the above in AA-resolution. However, there are some alternative pathways to speed up the simulations such as coarse grained (CG) MD simulations which can predict the phase behaviour of a multicomponent bilayer successfully[46-48] MARTINI-FF[49-50] is a very well-known CG-model that can correctly predict the phase behaviour or phase separation of a multicomponent membrane system. In MARTINI-FF four atoms in a lipid molecule is considered as one bead and thus it becomes possible to build larger systems and simulate it at longer time scales at low computational cost. However, for considering four atoms as a single bead CG-models are unable to distinguish lipids with 16:0 and 18:0 fatty acid chains. For water molecules we have taken the most commonly used CG-MARTINI water model[51] where one water bead is equivalent to four individual water molecules. In spite of such rough approximation, the dynamical properties (e.g., viscosity, diffusion coefficient) of CG water are in semiquantitative agreement[9] with the experiment[52-53]. Nonetheless, the freezing temperature of MARTINI-CG water is at around 290 K. Freezing of water at low temperature ranges can induce fluid-to-gel phase transition of the membrane. To prevent such undesiring freezing of water, anti-freeze particles[50, 54] are added (resembling the antifreezing agent). MARTINI

forcefield was originally parameterized at room temperature. But now, the MD simulations of realistic cell membranes are performed over a wide range of temperature[9, 55]. The earlier study has captured the temperature dependence of the diffusion and viscosity of MARTINI CG water in good agreement with the TIP4P/2005 water model[54]. Therefore, the MARTINI-CG water model is well enough for the simulation of realistic cell membrane at lower temperatures. The coarse-grained native E. coli membrane (NM) and modified E. coli membranes (MMS and MMU) are parameterised with recently optimised MARTINI 3 forcefield (www.cgmartini.nl). The equilibrated CG-NM membrane (193 lipids per leaflet) at 310 K is obtained from the website: https://github.com/KristynaPluhackova/MD_models_E. coli-PLE. After that it is multiplied four times using GROMACS. We have considered equal number of lipids in each leaflet. Henceforth, each leaflet contains 772 lipids. We have solvated the membrane with 38600 CG-water beads which is equivalent to 100 water molecules per lipid to keep the membrane fully hydrated. We have also added 480 Na ions (counter ions) for charge neutralisation. This is a reasonably larger system size to study the structure and phase behaviour of a complex multicomponent membrane system. To prevent the freezing of Martini CG-water at lower temperatures, 10% CG-water beads are replaced with antifreeze particles[56-57]. These antifreeze -particles does not interfere with the structure, fluidity, or phase behaviour of the lipid bilayer. The initial structure for MMS and MMU systems are taken from NM system and the forcefield for lipids are modified accordingly for the former two membranes. The martini bead containing cyclopropane ring is parameterised with the same bead type (C1) as for the saturated bead consistent with the literature[40] . To maintain the compatibility and universality, the bond lengths are kept unchanged: 0.47 nm for bonds within the hydrophobic tail and 0.51 nm for the bonds connecting glycerol and tail. But the angle containing cyclopropane ring in the middle is reparametrized to 125° with a harmonic constant of 15 kJ/mol/nm^2. For the MMS and MMU systems we have replaced the forcefield for CP containing lipids with its analogues

already available in martini website. For those which are not available, we have changed the angle from 125° to 180° and 125° to 120° for the single bond and double bond containing lipids in the middle respectively. In addition, the angle force constant is set to 35 kJ/mol/nm^2 for the corresponding single- or double bonds in MMS and MMU systems. C4 bead type is chosen for double bond containing beads.

All-atom modelling: Although the coarse-grained MD simulations of the solvated bio membrane systems are highly promising in spatio-temporal scales, it leads to loss of chemical details which are very important in quantitative study of various complex membrane systems, eg, molecular recognition for which atomistic details must remain[58-59] .Classical all-atom (AA) simulations can disclose the mechanism of several biological processes occurring in different length and time scales. Due to the availability of highly optimised atomistic forcefields we can explore the structure and dynamics of the biological membrane systems in realistic fashion and predict experimental results. The equilibrated structure of the AA-NM membrane at 310 K is obtained from the website: https://github.com/KristynaPluhackova/MD_models_E. coli-PLE. The initial structure of the MMS and MMU systems are generated with packmol software. Both the leaflets contain equal number of lipid molecules. We have taken 193 lipids per leaflet. The membranes are solvated with 16364 water molecules (around 42 water molecules per lipid, a reasonable hydration level for a fully hydrated system). We have also added 120 Na ions for charge neutralisation. NM, MMS and MMU membranes are parameterised with CHARMM36[60-61] all-atom forcefield since it provides the structure and dynamics in good agreement with the experimental data. The forcefield for the NM membrane lipids are obtained from literature. The MMS and MMU membrane lipid forcefields are obtained from CHARMM-GUI input generator[62-63]. For water molecules we have chosen CHARMM-modified TIP3P water model (also known as mTIP3P/TIPS3P). In the biomolecular simulations containing proteins or lipids the TIP3P and mTIP3P water models are more

accepted and appreciated over other models since CHARMM36 lipid forcefield is optimised with mTIP3P, and use of other water models may lead to inconsistencies in membrane properties used[61, 64]. Although the TIP4P model provides excellent results for the bulk water systems, it was not preferred for biomolecular simulations because it contains a virtual site and the forces must be projected on the "real" atoms. The mTIP3P water model has been selected since it reproduces the first shell hydration very well. In addition, most of the simulation time of solvated biomolecules is spent on simulating water molecules. Hence, a less costly mTIP3P model is favored[65].

2.3 Simulation Details

***CG-model-based simulation*:** GROMACS software package[66] is used for all CG-MARTINI simulations. After short energy minimization, the NM system is equilibrated for at least 2 μs followed by production run of 10 μs at 310 K. With the last configuration generated after production run, we have rapidly cooled the system to 250 K and equilibrated as a minimum for 10 μs (since at lower temperatures, systems take longer time to equilibrate). For MMS system even a longer simulation time of about 40 μs is required for equilibration. We gradually increased the temperature at 20K interval. Thus, we have simulated the NM, MMS and MMU membrane systems at 7 representative temperatures: 350, 330, 310, 300, 290, 270, and 250 K. The simulation lengths of different membrane systems are listed in Table S3. The v-rescale thermostat[67] is used for temperature coupling with a coupling constant of 1 ps. Pressure is controlled semiisotropically at 1 bar. Parrinello-Rahman barostat[68] is used for pressure coupling with a coupling constant of 12 ps and compressibility of 3×10^{-4} bar^{-1}. Position restraint is applied on the phosphate beads of each lipid along the z-direction in order to avoid unnecessary undulation of the larger membranes. It is observed in the earlier studies that memrane undulations can cause phase seperation in the bilayer membarne[69]. The real cell

membrane consists of transmembrane proteins which significantly reduce this sort of undulations[70]. However, in the present work, we have considered only the lipid membrane of an E. coli bacteria (without protien) and it is composed of 14 different type of lipids. Hence the membrane undulation can stimulate an unrealistic phase seperation which will impede the correct determination of the structural properties as well. Therfore, in the current work we have kept the membrane flat with weak position restraining. We have done the restraining with a harmonic force constant of 2 kJ mol^{-1} nm^{-2} applied on the phosphate beads of all of the lipids on the lower leaflet along the z-direction[9, 55]. Thus, both the local and global undulations of the membrane leaflets are inhibited. We have used the Verlet cutoff scheme with a Verlet-buffer-tolerance of 0.005 kJ/mol/ps. The van der Waals cutoff is set to 1.1nm using the potential-shift-Verlet method and coulomb cutoff is fixed to 1.1 nm. We have removed the centre-of-mass movement at every 100 steps.

AA-model-based simulation: AA-atom MD simulations are performed with GROMACS package. The already equilibrated NM membrane system, obtained from literature is directly simulated at 310K for 230 ns. After short energy minimization using the steepest-descent algorithm, the MMS and MMU systems are equilibrated at 310 K at least for 100 ns followed by production run of 100 ns. We gradually cooled the three membrane systems (NM, MMS, and MMU) from 310K to 250K with the last configuration obtained after production run at 310 K. Cooling is done via annealing with 1 K/ns rate. Then we equilibrated each system not less than 250 ns, as molecules takes longer time to diffuse at lower temperature, hence longer time is required to reach the equilibrium. The temperature is increased gradually at 20 K interval. All the membranes are simulated at 6 different temperatures: 350, 330, 310, 290, 270, and 250K. The simulation lengths of different membrane systems are listed in Table S3. All the simulations are performed using NPT ensemble. Nose-Hoover thermostat[71-72] with a coupling constant of 0.5 ps is used for temperature coupling. The pressure is controlled

semiisotropically. Berendsen barostat[73] is used for pressure coupling with a coupling constant of 5 ps. Periodic boundary conditions are applied in all three directions. Verlet leapfrog algorithm is used for solving the equations of motion at every 2 fs. Long-range electrostatic interactions are solved with the Particle Mesh Ewald (PME) summation method. The cut-off for the short-range Coulomb interactions and van der Waals interactions are set to 1.2 nm. The hydrogen containing bonds are constrained with lincs algorithm.

3. RESULTS AND DISCUSSIONS

3.1. Coarse-grained (CG) Simulation

We first examine the packing density parameters — area per lipid $\langle A_L \rangle$, membrane thickness $\langle T_L \rangle$, volume per lipid $\langle V_L \rangle$ — and fluidity parameters — lateral diffusion coefficient D_{xy} and rotational auto-correlation function (RCF) — of three membrane systems NM, MMS, and MMU from CG resolution. (The methods for calculating the above properties are described in Section 2 of SI.) Figure 1a shows that with decreasing temperature, $\langle A_L \rangle$ and $\langle V_L \rangle$ decrease, while $\langle T_L \rangle$ increases almost linearly for both the NM and MMU membranes. The membrane fluidity, gauged by D_{xy} (Figure 1a) and RCF decay (Figure S6 of SI), constantly decreases with decreasing temperature. These suggest an absence of fluid-to-gel phase transition within the temperature range. Notably, the values for both NM and MMU almost coincide with each other at all temperatures. Therefore, the CG model is unable to distinguish between NM and MMU membranes and therefore the purpose of cyclopropanation is not clear. However, for MMS we observe a drastic change of all the quantities below 300 K strongly suggesting fluid-to-gel phase transition. Therefore, the adverse effect of cooling on membrane with saturated lipids instead of cyclopropane or unsaturated lipids is clear.

To provide more insight into the spatial arrangement of the lipids in *xy*-plane we present, in Figure 1b, the lateral density profiles (LDP) of lipids in the three membranes NM,

MMU, and MMS at 250 K. It is observed that the NM and MMU membranes remain fluid, while the MMS is gel at 250 K, consistent with the drastic changes in the packing density and fluidity between 290 and 300 K (see Figure 1a). Closer inspection reveals that a small portion of the MMS membrane remains fluid. As shown in Figure 1c, this fluid domain is mainly composed of mono- and di-unsaturated lipids. The Voronoi-based spatial profiles[74] of membrane thickness at different temperatures (Figure 1d) shows that the size of the fluid domain increases with increasing temperature such that at 300 K the membrane becomes entirely fluid. Figure 1e presents the area per lipid and thickness values for different lipids, grouped by the type of acyl chain (cyclopropane ring containing, unsaturated, and fully saturated). Clearly, for NM, all lines coincide with each other suggesting a uniformity in the cooling response of the lipids. On the other hand, for MMS, the saturated lipids respond more strongly towards cooling than the unsaturated lipids. This is due to the closer packing of saturated lipids than the unsaturated lipids. In MMU membrane the tri-unsaturated lipids occupy more area although the thickness is same throughout the lipid types. In brief, Figure 1 indicates that cyclopropane rings in the lipid acyl chains maintain packing density and fluidity of the cell membrane of E. coli very similar to what unsaturated acyl chain containing lipid does. However, the specific purpose of cyclopropanation of the lipid acyl chain is not clear from the CG resolution. The area and thickness of lipids with different headgroups are not distinguishable from each other from the present CG-based simulation (see Figures S2-S3).

3.2. All-atom Simulation

Since the CG-based models are inadequate to differentiate between the membranes with unsaturated and cyclopropane ring containing lipids, we simulate three membranes (NM, MMS, and MMU) under all-atom (AA) resolution. The results obtained from AA-simulations are depicted in Figure 2. Figures 2a-b display the temperature dependence of average area per lipid $<A_L>$ and average membrane thickness $<T_L>$. Figures 2c-d show average deuterium order

parameter $<S_{CD}>$ for different categories of acyl chains (cyclopropane ring-, monounsaturated chain-, and saturated chain-containing). The above results indicate that the NM membrane shows the least change of the packing density on cooling, while the MMS membrane exhibits a sharp change between 310 and 330K due to the fluid-to-gel phase transition. However, all the changes are less dramatic compared to that in CG-resolution, which indicates a partial gel formation of the MMS membrane. More interestingly, a clear difference in the packing densities between the NM and MMU membranes is now vivid. The MMU membrane undergoes relatively sharp transition between 290 and 270 K. The structural parameters portray some ordering in MMU bilayer compared to NM and the difference is more visible below 290 K. However, the dynamics of the lipid membrane is less impacted by replacing the cyclopropane rings with C-C single bond or C=C double bond. The lateral diffusion coefficient (D_{xy}) values for the NM and MMU practically merge with each other, while the MMS is twice less diffusive. Unlike the diffusion coefficient, the short time membrane fluidity which can be denoted by the rotational auto-correlation function (RCF) (Figures 2f-h) is bit more impacted under the above conditions. The RCF decay slows down with cooling. While at 350 K the correlations decay at the same rate for all three membranes, at the lower temperatures (<270 K) the order of slowing down of RCF decay is MMS > MMU > NM.

It is known that the occurrence of kinks in the acyl chains impede close packing of the lipids and thereby retain the membrane fluidity at lower temperature[7-9, 29, 31] . Such kinks are provided by the presence of cyclopropane rings or C=C double bonds in the acyl chains. The key focus is to reveal which sort of kinks are more rigid to disrupt the packing or more precisely the ordering of the lipid bilayer. We have considered the three types of acyl chains (cyclopropane ring-, monounsaturated chain-, and saturated chain-containing), as taken in the calculation of $<S_{CD}>$. The kink angle is calculated using the vectors shown in Figure 3b. The kink angle distributions, presented in Figure 3a for various temperatures, show that the kink of

a cyclopropane containing acyl chain in NM is not perturbed by the cold shock. They also do not allow other saturated and monounsaturated fatty acid chains to align themselves in an ordered arrangement. On the other hand, in both MMU and MMS, the kink angle sharply increases below a certain temperature for the saturated and monounsaturated chains. The higher kink rigidity of the cyclopropane containing fatty acid chain introduces the packing defects which in turn hinder the gel phase formation. The presence of cyclopropane rings not only inhibit the phase transition of the LCFAs, but also avert the same for the LSFAs and LUFAs in the NM system. Therefore, the cyclopropane rings are more effective than C=C double bonds to prevent the phase transition of the lipids from fluid to gel phase at lower temperature

Apart from kink angle, dihedral angle distributions are also relevant to provide an overall understanding about the stability of various structural conformations of the lipid acyl chains. The highest peak of the distribution specifies the most probable conformation. Since in realistic bacterial membranes -cis conformations are most abundant, in the present study, only -cis geometry of the double bond or cyclopropane (CP) rings are considered. The CP rings or double bonds are located nearly in the mid position of the acyl chains for the three membrane systems. For each acyl chain, we have calculated the distributions of dihedral angles: φ_9, φ_{10}, and φ_{11} at three representative temperatures: 250, 310, and 350 K (Figure 4). For both cyclopropane and C=C containing chains a sharp peak is observed at 0^o (φ_{10}). The -cis geometry forces the C8 and C11 carbons to stay at 0^o for both the chains. The C9 and C10 carbons are sp^2 hybridized for the monounsaturated chains. Hence, straightening of the chains at lower temperature (250 K) promotes high strain on the C=C double bond. Similar effect is observed for the cyclopropane ring system also. Here, although the C9 and C10 carbons of the CP rings are sp^3 hybridized, the highly strained ring structure does not facilitate the twisting of the C-C single bonds (C8, C9 and C10, C11), which in turn gives rise to a sharp peak at 0^o. For the monounsaturated chains we observe two minor peaks at 120^o for the φ_9 and φ_{11} dihedrals.

The symmetric nature of the peaks suggests the equivalency of the two dihedrals. In contrast, the peaks for φ_9 and φ_{11} are not symmetrical for the cyp chains indicating that although these two dihedrals look similar, they are non-equivalent and we find peaks near 90^o and 180^o. With lowering of temperature peak height increases, confirming a more rigidity of the acyl chains against twisting. The dihedral distribution for the sat. chains show a peak-maxima at 180^o and two symmetric minor peaks at 60^o. We have observed that the anti-geometry (180^o) is more favorable than gauche (60^o) and the later follows a reverse trend in peak distribution with reducing temperature. Hence, we can infer, the bending of the sat. chains are more probable at higher temperatures indicating the fluid phase of the membrane bilayer. Nonetheless, the temperature dependence of the peak height is more visible for the sat. chains compare to cyp. or monounsat. analogues. The order of increasing probability of the sat. chains at 250 K is: NM < MMU < MMS, which indicates that the presence of CP rings unfavor the straightening of the sat. chains more than C=C double bonds and thereby suppress the close-packing of the lipids to form gel. However, the dihedral angles of the monounsat. chains are not much affected by the presence of CP rings or fully saturated chains.

We have seen that on cooling the LCFAs neither undergoes phase transition themselves nor do they allow other lipids to have phase transition. Even the fully saturated LSFAs, present in NM, also behave very similar to the LCFAs. This is intriguing and needs further investigation. Separation of phases is a prevalent phenomenon, highly being observed in the multicomponent membrane systems. It arises due to the sufficiently large structural differences of the lipids, inducing unfavorable interactions among them. Therefore, one can expect the LCFAs, with highly kinked fatty acid chains, to phase separate from the remaining lipids. We have analyzed the distribution of different kinds of lipid inside the membrane at the lowest temperature (250 K) and how their phase behavior is impacted. We have shown the lateral density profile (LDP) of the bilayer for different membrane systems at 250 K averaged over

two time frames (Figure 5a). We have also picturized the distribution of different sorts of lipids based on saturation level and presence of cyclopropane rings in acyl chains at the same temperature (Figure 5b). We observe that for the NM membrane, the distinct types of lipids are homogeneously distributed in the membrane systems. Some transient domain formation is observed but complete phase separation of the lipids is still absent. Therefore, the LCFAs are fully mixed with other lipids and thereby inhibits phase transition of the latter. Side-by-side comparison between the 2D-densmap (Figure 5a) and a simulation snapshot (Figure 5b) reveals that in NM the LCFA-rich regions are more fluidic compared to the regions having the monounsaturated lipids. The LSFA-rich regions in MMS undergoes gel phase, while some fluidity is observed near the LUFA-rich regions. Interestingly, the monounsaturated lipids in MMU undergoes fluid-to-gel phase transition, while the di- and tri-unsaturated lipids are fluidic and a fluid-gel phase separation is clearly observed. Similar phase separation is not observed in NM.

The Voronoi-based analysis of the area per lipid (Figure S9 of SI) and membrane thickness (Figure 5c) for different types of lipids, depending on saturation level and presence of CP rings show that for the MMS and MMU systems sharp changes in thickness at the phase transition temperatures (310 K for MMS and 270K for MMU) are observed. There are clear differences between the saturated, mono-, di, and tri-unsaturated lipids near the phase transition point for the above modified membranes. The saturated lipids show the sharpest change at the phase transition point followed by monounsaturated and di-unsaturated lipids. On the other hand, absolutely no changes are observed between cyclopropane ring-containing, mono-, and di-unsaturated lipids and the values practically merges with each other in the NM system. Therefore, the LCFAs homogenize the membrane composition.

The above homogenization by the LCFAs and mutual interactions between the different kinds of lipids are shown via cluster size analysis and radial distribution functions $g(r)$. We

have performed lipid cluster size analysis of the membranes from both CG (Figure S4 and S5 of SI) and AA resolutions (Figure S7 of SI). Evidently, the lipids do not tend to form bigger clusters and the cluster size increases slightly with decreasing temperature. Further to understand the specific interactions between lipids we have calculated $g(r)$ between the same and different kinds of lipids (Figure S8 of SI) in the same membrane leaflet from AA resolution. It manifests, how different types of lipids interact among each other and predicts the possibility of phase separation assisted phase transition[9]. The most abundant lipids of a particular membrane system are only considered. For the NM and MMS systems, we notice, with decrease in temperature, peak height of $g(r)$ increases for all types of lipids (Figure 5d) which suggests the same and different kinds of lipids equally interact with each other, giving rise to a homogenous distribution of lipids inside the membrane. On the other hand, in MMU system, same type of lipids interact more strongly among each other in comparison to the different types of lipids. This indicates a partial phase separation between the monounsaturated and di-unsaturated lipids in the MMU membrane, which induces fluid-to-gel phase transition. Hence, the cyclopropane rings not only inhibit the cooling induced phase transition of the cyclopropane containing lipids, but also protects other lipids from the deleterious effect of cold shock.

5. CONCLUSION

In conclusion, the present work manifests the role of cyclopropane rings towards the survival of E. coli bacteria during cold shock. We have simulated a realistic lipid bilayer of an E. coli bacteria along with the modified membranes, replacing the cyclopropane rings either with single or double bonds in both CG and AA resolutions. The simulations are performed at various temperatures between 250 and 350 K. There is hardly any difference between the impact of cyclopropane ring and double bond over the structural and dynamical properties of the membrane in CG resolution, which indicates the insufficiency of the CG model of cyclopropane containing lipids to explain the membrane properties. Nevertheless, in all-atom

resolution, we have obtained visible difference in membrane properties due to the presence of cyclopropane ring and unsaturation specifically at lower temperatures. Notably, the cyclopropane rings are more effective to restrict the closer packing of the membrane lipids compared to double bonds by providing a rigid kink along the acyl chain. In addition, cyclopropane rings not only prevent the fluid-to-gel phase transformation of the corresponding lipids, but also inhibits the phase transition of the unsaturated lipids as well by interacting with all different lipids present in the membrane. Therefore, this study provides an explanation on why the E. coli bacterial strain, susceptible to freezing environment, relies on the cyclopropanation of the acyl chain-double bond. Similar explanation may also be equally applicable for other bacteria, adopting cyclopropanation as cell-survival strategy.

6. ASSOCIATED CONTENT

Supporting Information

The Supporting Information (SI) is available free of charge at___. The SI contains four sections. S1. consists of composition of the membrane; S2. contains method of analysis; S3. includes additional CG-results; S4. contains additional AA-results.

7. AUTHOR INFORMATION

Corresponding Author
Snehasis Daschakraborty − Department of Chemistry, Indian Institute of Technology Patna, Patna, Bihar 801106, India; orcid.org/0000-0002-2694-7142; Email: snehasis@iitp.ac.in

Author
Archita Maiti − Department of Chemistry, Indian Institute of Technology Patna, Patna, Bihar 801106, India;

Abhay Kumar − Department of Chemistry, Indian Institute of Technology Patna, Patna, Bihar 801106, India;

Notes
The authors declare no competing financial interest.

8. ACKNOWLEDGEMENTS

We acknowledge the Council of Scientific and Industrial Research (CSIR) for funding (Scheme No. 01(3056)/21/EMRII) and IIT Patna for the computational facility. A. M. acknowledges IIT Patna and A. K. acknowledges UGC for their research fellowships.

9. REFERENCES

1. Mansilla, M. C.; Cybulski, L. E.; Albanesi, D.; de Mendoza, D., Control of membrane lipid fluidity by molecular thermosensors. *Journal of bacteriology* **2004,** *186* (20), 6681-8.
2. Mihoub, F.; Mistou, M. Y.; Guillot, A.; Leveau, J. Y.; Boubetra, A.; Billaux, F., Cold adaptation of Escherichia coli: microbiological and proteomic approaches. *International journal of food microbiology* **2003,** *89* (2-3), 171-84.
3. Maiti, A.; Daschakraborty, S., Effect of TMAO on the Structure and Phase Transition of Lipid Membranes: Potential Role of TMAO in Stabilizing Cell Membranes under Osmotic Stress. *The journal of physical chemistry. B* **2021,** *125* (4), 1167-1180.
4. Quinn, P. J., A lipid-phase separation model of low-temperature damage to biological membranes. *Cryobiology* **1985,** *22* (2), 128-46.
5. Williams, W. P.; Chapman, D.; Heber, U.; Franks, F.; Jaenicke, R.; Laws, R. M.; Franks, F., Cold-induced lipid phase transitions. *Philosophical Transactions of the Royal Society of London. B, Biological Sciences* **1990,** *326* (1237), 555-570.
6. Drobnis, E. Z.; Crowe, L. M.; Berger, T.; Anchordoguy, T. J.; Overstreet, J. W.; Crowe, J. H., Cold shock damage is due to lipid phase transitions in cell membranes: A demonstration using sperm as a model. *Journal of Experimental Zoology* **1993,** *265* (4), 432-437.
7. Ernst, R.; Ejsing, C. S.; Antonny, B., Homeoviscous Adaptation and the Regulation of Membrane Lipids. *Journal of molecular biology* **2016,** *428* (24 Pt A), 4776-4791.
8. Sinensky, M., Homeoviscous adaptation--a homeostatic process that regulates the viscosity of membrane lipids in Escherichia coli. *Proceedings of the National Academy of Sciences of the United States of America* **1974,** *71* (2), 522-5.
9. Erimban, S.; Daschakraborty, S., Cryostabilization of the Cell Membrane of a Psychrotolerant Bacteria via Homeoviscous Adaptation. *The Journal of Physical Chemistry Letters* **2020,** *11* (18), 7709-7716.
10. Weber, M. H.; Klein, W.; Müller, L.; Niess, U. M.; Marahiel, M. A., Role of the Bacillus subtilis fatty acid desaturase in membrane adaptation during cold shock. *Molecular microbiology* **2001,** *39* (5), 1321-9.
11. Nichols, D. S.; Miller, M. R.; Davies, N. W.; Goodchild, A.; Raftery, M.; Cavicchioli, R., Cold adaptation in the Antarctic Archaeon Methanococcoides burtonii involves membrane lipid unsaturation. *Journal of bacteriology* **2004,** *186* (24), 8508-15.
12. Beranová, J.; Jemioła-Rzemińska, M.; Elhottová, D.; Strzałka, K.; Konopásek, I., Metabolic control of the membrane fluidity in Bacillus subtilis during cold adaptation. *Biochimica et biophysica acta* **2008,** *1778* (2), 445-53.
13. Fukunaga, N.; Russell, N. J., Membrane lipid composition and glucose uptake in two psychrotolerant bacteria from Antarctica. *Microbiology* **1990,** *136* (9), 1669-1673.
14. Männistö, M. K.; Puhakka, J. A., Temperature- and growth-phase-regulated changes in lipid fatty acid structures of psychrotolerant groundwater Proteobacteria. *Archives of microbiology* **2001,** *177* (1), 41-6.

15. Bajerski, F.; Wagner, D.; Mangelsdorf, K., Cell Membrane Fatty Acid Composition of Chryseobacterium frigidisoli PB4(T), Isolated from Antarctic Glacier Forefield Soils, in Response to Changing Temperature and pH Conditions. *Frontiers in microbiology* **2017,** *8*, 677.
16. Sohlenkamp, C.; Geiger, O., Bacterial membrane lipids: diversity in structures and pathways. *FEMS microbiology reviews* **2016,** *40* (1), 133-59.
17. Tookmanian, E. M.; Belin, B. J.; Sáenz, J. P.; Newman, D. K., The role of hopanoids in fortifying rhizobia against a changing climate. *Environmental microbiology* **2021,** *23* (6), 2906-2918.
18. Ballweg, S.; Sezgin, E.; Doktorova, M.; Covino, R.; Reinhard, J.; Wunnicke, D.; Hänelt, I.; Levental, I.; Hummer, G.; Ernst, R., Regulation of lipid saturation without sensing membrane fluidity. *Nat Commun* **2020,** *11* (1), 756.
19. Chwastek, G.; Surma, M. A.; Rizk, S.; Grosser, D.; Lavrynenko, O.; Rucińska, M.; Jambor, H.; Sáenz, J., Principles of Membrane Adaptation Revealed through Environmentally Induced Bacterial Lipidome Remodeling. *Cell Rep* **2020,** *32* (12), 108165.
20. Maiti, A.; Daschakraborty, S., How Do Urea and Trimethylamine N-Oxide Influence the Dehydration-Induced Phase Transition of a Lipid Membrane? *The journal of physical chemistry. B* **2021,** *125* (36), 10149-10165.
21. Maiti, A.; Daschakraborty, S., Can Urea and Trimethylamine-N-oxide Prevent the Pressure-Induced Phase Transition of Lipid Membrane? *The Journal of Physical Chemistry B* **2022,** *126* (7), 1426-1440.
22. Harries, D.; Rösgen, J., A practical guide on how osmolytes modulate macromolecular properties. *Methods in cell biology* **2008,** *84*, 679-735.
23. Pham, Q. D.; Wolde-Kidan, A.; Gupta, A.; Schlaich, A.; Schneck, E.; Netz, R. R.; Sparr, E., Effects of Urea and TMAO on Lipid Self-Assembly under Osmotic Stress Conditions. *The journal of physical chemistry. B* **2018,** *122* (25), 6471-6482.
24. Nowacka, A.; Douezan, S.; Wadsö, L.; Topgaard, D.; Sparr, E., Small polar molecules like glycerol and urea can preserve the fluidity of lipid bilayers under dry conditions. *Soft matter* **2012,** *8* (5), 1482-1491.
25. Kosar, F.; Akram, N. A.; Sadiq, M.; Al-Qurainy, F.; Ashraf, M., Trehalose: a key organic osmolyte effectively involved in plant abiotic stress tolerance. *Journal of Plant Growth Regulation* **2019,** *38* (2), 606-618.
26. Nishiguchi, M. K.; Somero, G. N., Temperature- and concentration-dependence of compatibility of the organic osmolyte beta-dimethylsulfoniopropionate. *Cryobiology* **1992,** *29* (1), 118-24.
27. Vereyken, I. J.; Chupin, V.; Islamov, A.; Kuklin, A.; Hincha, D. K.; de Kruijff, B., The effect of fructan on the phospholipid organization in the dry state. *Biophysical journal* **2003,** *85* (5), 3058-65.
28. Leslie, S. B.; Israeli, E.; Lighthart, B.; Crowe, J. H.; Crowe, L. M., Trehalose and sucrose protect both membranes and proteins in intact bacteria during drying. *Appl Environ Microbiol* **1995,** *61* (10), 3592-7.
29. Zhang, Y.-M.; Rock, C. O., Membrane lipid homeostasis in bacteria. *Nature Reviews Microbiology* **2008,** *6* (3), 222-233.
30. Velly, H.; Bouix, M.; Passot, S.; Penicaud, C.; Beinsteiner, H.; Ghorbal, S.; Lieben, P.; Fonseca, F., Cyclopropanation of unsaturated fatty acids and membrane rigidification improve the freeze-drying resistance of Lactococcus lactis subsp. lactis TOMSC161. *Applied microbiology and biotechnology* **2015,** *99* (2), 907-18.
31. Poger, D.; Mark, A. E., A Ring to Rule Them All: The Effect of Cyclopropane Fatty Acids on the Fluidity of Lipid Bilayers. *The Journal of Physical Chemistry B* **2015,** *119* (17), 5487-5495.

32. Grogan, D. W.; Cronan, J. E., Jr., Cyclopropane ring formation in membrane lipids of bacteria. *Microbiology and molecular biology reviews : MMBR* **1997,** *61* (4), 429-41.
33. Kim, B. H.; Kim, S.; Kim, H. G.; Lee, J.; Lee, I. S.; Park, Y. K., The formation of cyclopropane fatty acids in Salmonella enterica serovar Typhimurium. *Microbiology (Reading, England)* **2005,** *151* (Pt 1), 209-218.
34. Hyono, A.; Kuriyama, S.; Hara, H.; Yano, I.; Masui, M., ESR studies on the membrane properties of a moderately halophilic bacterium. I. Physical properties of lipid bilayers in whole cells. *Journal of biochemistry* **1980,** *88* (5), 1267-74.
35. Annous, B. A.; Kozempel, M. F.; Kurantz, M. J., Changes in membrane fatty acid composition of Pediococcus sp. strain NRRL B-2354 in response to growth conditions and its effect on thermal resistance. *Applied and environmental microbiology* **1999,** *65* (7), 2857-62.
36. Hari, S. B.; Grant, R. A.; Sauer, R. T., Structural and Functional Analysis of E. coli Cyclopropane Fatty Acid Synthase. *Structure* **2018,** *26* (9), 1251-1258.e3.
37. Furse, S.; Wienk, H.; Boelens, R.; de Kroon, A. I. P. M.; Killian, J. A., E. coli MG1655 modulates its phospholipid composition through the cell cycle. *FEBS Letters* **2015,** *589* (19, Part B), 2726-2730.
38. Chang, Y. Y.; Cronan, J. E., Jr., Membrane cyclopropane fatty acid content is a major factor in acid resistance of Escherichia coli. *Molecular microbiology* **1999,** *33* (2), 249-59.
39. Nickels, J. D.; Chatterjee, S.; Mostofian, B.; Stanley, C. B.; Ohl, M.; Zolnierczuk, P.; Schulz, R.; Myles, D. A. A.; Standaert, R. F.; Elkins, J. G.; Cheng, X.; Katsaras, J., Bacillus subtilis Lipid Extract, A Branched-Chain Fatty Acid Model Membrane. *The Journal of Physical Chemistry Letters* **2017,** *8* (17), 4214-4217.
40. Pluhackova, K.; Horner, A., Native-like membrane models of E. coli polar lipid extract shed light on the importance of lipid composition complexity. *BMC Biology* **2021,** *19* (1), 4.
41. Shi, Q.; Voth, G. A., Multi-Scale Modeling of Phase Separation in Mixed Lipid Bilayers. *Biophysical journal* **2005,** *89* (4), 2385-2394.
42. Lu, L.; Voth, G. A., Systematic Coarse-graining of a Multicomponent Lipid Bilayer. *The Journal of Physical Chemistry B* **2009,** *113* (5), 1501-1510.
43. Marrink, S. J.; Corradi, V.; Souza, P. C. T.; Ingólfsson, H. I.; Tieleman, D. P.; Sansom, M. S. P., Computational Modeling of Realistic Cell Membranes. *Chemical reviews* **2019,** *119* (9), 6184-6226.
44. Leonard, A. N.; Wang, E.; Monje-Galvan, V.; Klauda, J. B., Developing and Testing of Lipid Force Fields with Applications to Modeling Cellular Membranes. *Chemical reviews* **2019,** *119* (9), 6227-6269.
45. Pluhackova, K.; Böckmann, R. A., Biomembranes in atomistic and coarse-grained simulations. *Journal of physics. Condensed matter : an Institute of Physics journal* **2015,** *27* (32), 323103.
46. Marrink, S. J.; Tieleman, D. P., Perspective on the Martini model. *Chemical Society Reviews* **2013,** *42* (16), 6801-6822.
47. Periole, X.; Marrink, S. J., The Martini coarse-grained force field. *Methods in molecular biology (Clifton, N.J.)* **2013,** *924*, 533-65.
48. Ingólfsson, H. I.; Lopez, C. A.; Uusitalo, J. J.; de Jong, D. H.; Gopal, S. M.; Periole, X.; Marrink, S. J., The power of coarse graining in biomolecular simulations. *Wiley interdisciplinary reviews. Computational molecular science* **2014,** *4* (3), 225-248.
49. Marrink, S. J.; Risselada, H. J.; Yefimov, S.; Tieleman, D. P.; de Vries, A. H., The MARTINI force field: coarse grained model for biomolecular simulations. *The journal of physical chemistry. B* **2007,** *111* (27), 7812-24.
50. Marrink, S. J.; de Vries, A. H.; Mark, A. E., Coarse Grained Model for Semiquantitative Lipid Simulations. *The Journal of Physical Chemistry B* **2004,** *108* (2), 750-760.

51. Souza, P. C. T.; Alessandri, R.; Barnoud, J.; Thallmair, S.; Faustino, I.; Grünewald, F.; Patmanidis, I.; Abdizadeh, H.; Bruininks, B. M. H.; Wassenaar, T. A.; Kroon, P. C.; Melcr, J.; Nieto, V.; Corradi, V.; Khan, H. M.; Domański, J.; Javanainen, M.; Martinez-Seara, H.; Reuter, N.; Best, R. B.; Vattulainen, I.; Monticelli, L.; Periole, X.; Tieleman, D. P.; de Vries, A. H.; Marrink, S. J., Martini 3: a general purpose force field for coarse-grained molecular dynamics. *Nature methods* **2021,** *18* (4), 382-388.
52. Price, W. S.; Ide, H.; Arata, Y., Self-Diffusion of Supercooled Water to 238 K Using PGSE NMR Diffusion Measurements. *The Journal of Physical Chemistry A* **1999,** *103* (4), 448-450.
53. Dehaoui, A.; Issenmann, B.; Caupin, F., Viscosity of deeply supercooled water and its coupling to molecular diffusion. *Proceedings of the National Academy of Sciences* **2015,** *112* (39), 12020-12025.
54. Baoukina, S.; Rozmanov, D.; Tieleman, D. P., Composition Fluctuations in Lipid Bilayers. *Biophys J* **2017,** *113* (12), 2750-2761.
55. Erimban, S.; Daschakraborty, S., Homeoviscous Adaptation of the Lipid Membrane of a Soil Bacterium Surviving under Diurnal Temperature Variation: A Molecular Simulation Perspective. *The Journal of Physical Chemistry B* **2022,** *126* (39), 7638-7650.
56. Jaschonek, S.; Cascella, M.; Gauss, J.; Diezemann, G.; Milano, G., Intramolecular structural parameters are key modulators of the gel-liquid transition in coarse grained simulations of DPPC and DOPC lipid bilayers. *Biochemical and biophysical research communications* **2018,** *498* (2), 327-333.
57. Patel, L. A.; Kindt, J. T., Coarse-grained molecular simulations of the melting kinetics of small unilamellar vesicles. *Soft Matter* **2016,** *12* (6), 1765-1777.
58. Kar, P.; Feig, M., Hybrid All-Atom/Coarse-Grained Simulations of Proteins by Direct Coupling of CHARMM and PRIMO Force Fields. *J Chem Theory Comput* **2017,** *13* (11), 5753-5765.
59. Hollingsworth, S. A.; Dror, R. O., Molecular Dynamics Simulation for All. *Neuron* **2018,** *99* (6), 1129-1143.
60. Klauda, J. B.; Venable, R. M.; Freites, J. A.; O'Connor, J. W.; Tobias, D. J.; Mondragon-Ramirez, C.; Vorobyov, I.; MacKerell, A. D., Jr.; Pastor, R. W., Update of the CHARMM All-Atom Additive Force Field for Lipids: Validation on Six Lipid Types. *The Journal of Physical Chemistry B* **2010,** *114* (23), 7830-7843.
61. Pastor, R. W.; Mackerell, A. D., Jr., Development of the CHARMM Force Field for Lipids. *J Phys Chem Lett* **2011,** *2* (13), 1526-1532.
62. Jo, S.; Kim, T.; Iyer, V. G.; Im, W., CHARMM-GUI: A web-based graphical user interface for CHARMM. *Journal of Computational Chemistry* **2008,** *29* (11), 1859-1865.
63. Lee, J.; Cheng, X.; Swails, J. M.; Yeom, M. S.; Eastman, P. K.; Lemkul, J. A.; Wei, S.; Buckner, J.; Jeong, J. C.; Qi, Y.; Jo, S.; Pande, V. S.; Case, D. A.; Brooks, C. L., III; MacKerell, A. D., Jr.; Klauda, J. B.; Im, W., CHARMM-GUI Input Generator for NAMD, GROMACS, AMBER, OpenMM, and CHARMM/OpenMM Simulations Using the CHARMM36 Additive Force Field. *Journal of Chemical Theory and Computation* **2016,** *12* (1), 405-413.
64. Piggot, T. J.; Piñeiro, Á.; Khalid, S., Molecular Dynamics Simulations of Phosphatidylcholine Membranes: A Comparative Force Field Study. *Journal of chemical theory and computation* **2012,** *8* (11), 4593-609.
65. MacKerell, A. D., Jr.; Bashford, D.; Bellott, M.; Dunbrack, R. L., Jr.; Evanseck, J. D.; Field, M. J.; Fischer, S.; Gao, J.; Guo, H.; Ha, S.; Joseph-McCarthy, D.; Kuchnir, L.; Kuczera, K.; Lau, F. T. K.; Mattos, C.; Michnick, S.; Ngo, T.; Nguyen, D. T.; Prodhom, B.; Reiher, W. E.; Roux, B.; Schlenkrich, M.; Smith, J. C.; Stote, R.; Straub, J.; Watanabe, M.; Wiórkiewicz-Kuczera, J.; Yin, D.; Karplus, M., All-Atom Empirical Potential for Molecular Modeling and

Dynamics Studies of Proteins. *The Journal of Physical Chemistry B* **1998,** *102* (18), 3586-3616.
66. Van Der Spoel, D.; Lindahl, E.; Hess, B.; Groenhof, G.; Mark, A. E.; Berendsen, H. J., GROMACS: fast, flexible, and free. *J Comput Chem* **2005,** *26* (16), 1701-18.
67. Bussi, G.; Donadio, D.; Parrinello, M., Canonical sampling through velocity rescaling. *The Journal of Chemical Physics* **2007,** *126* (1), 014101.
68. Parrinello, M.; Rahman, A., Polymorphic transitions in single crystals: A new molecular dynamics method. *Journal of Applied Physics* **1981,** *52* (12), 7182-7190.
69. Ingólfsson, H. I.; Carpenter, T. S.; Bhatia, H.; Bremer, P. T.; Marrink, S. J.; Lightstone, F. C., Computational Lipidomics of the Neuronal Plasma Membrane. *Biophys J* **2017,** *113* (10), 2271-2280.
70. Duncan, A. L.; Reddy, T.; Koldsø, H.; Hélie, J.; Fowler, P. W.; Chavent, M.; Sansom, M. S. P., Protein crowding and lipid complexity influence the nanoscale dynamic organization of ion channels in cell membranes. *Scientific Reports* **2017,** *7* (1), 16647.
71. Hoover, W. G., Canonical dynamics: Equilibrium phase-space distributions. *Physical review. A, General physics* **1985,** *31* (3), 1695-1697.
72. Nosé, S., A unified formulation of the constant temperature molecular dynamics methods. *The Journal of Chemical Physics* **1984,** *81* (1), 511-519.
73. Berendsen, H. J. C.; Postma, J. P. M.; van Gunsteren, W. F.; DiNola, A.; Haak, J. R., Molecular dynamics with coupling to an external bath. *The Journal of Chemical Physics* **1984,** *81* (8), 3684-3690.
74. Lukat, G.; Krüger, J.; Sommer, B., APL@Voro: A Voronoi-Based Membrane Analysis Tool for GROMACS Trajectories. *Journal of Chemical Information and Modeling* **2013,** *53* (11), 2908-2925.

Figures

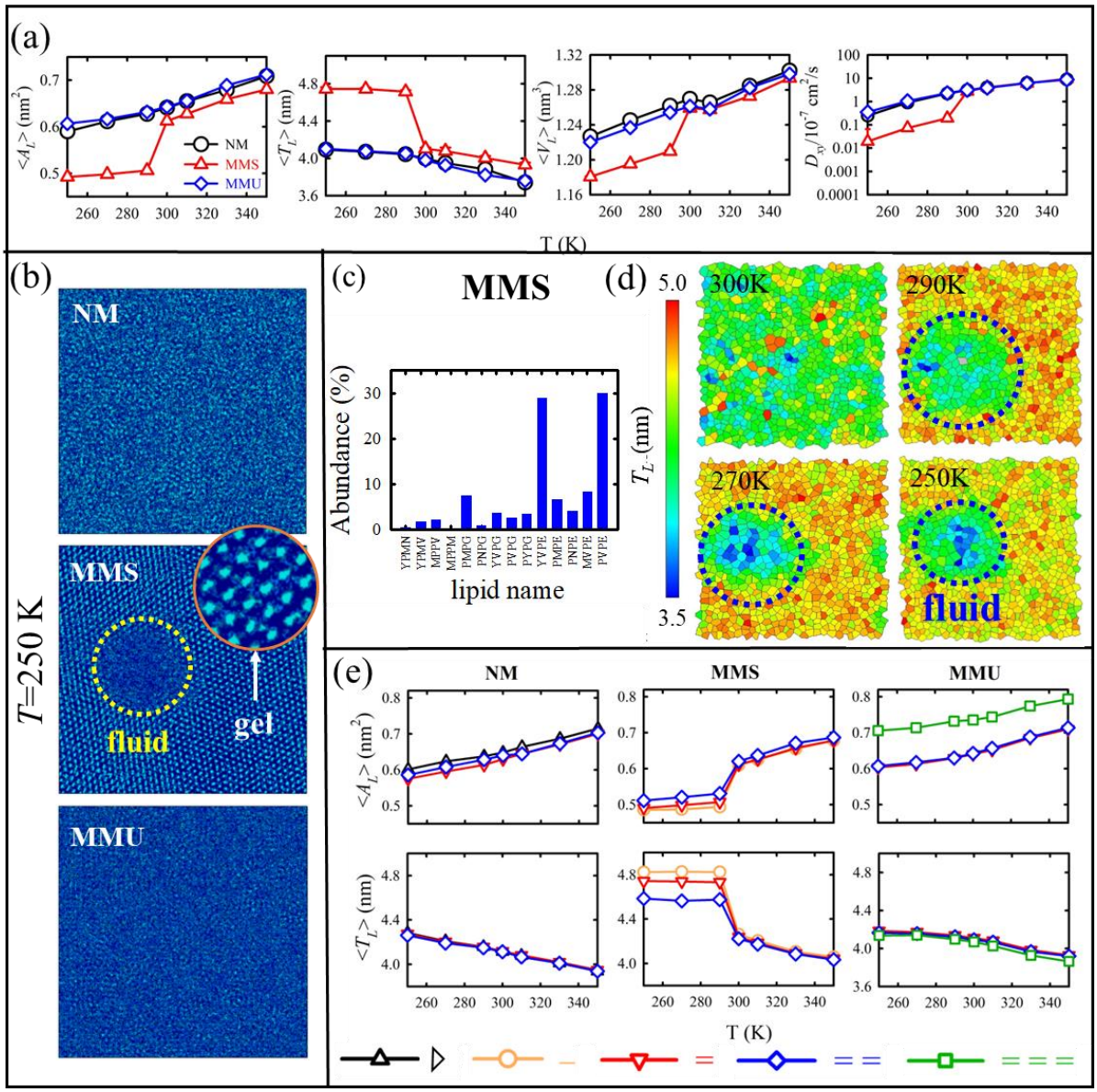

Figure 1. (a) Area per lipid <A_L>, membrane thickness <T_L>, volume per lipid <V_L>, and lateral diffusion coefficient D_{xy} as a function of temperature for the NM (black), MMS (red), and MMU (blue) systems. (b) 2D-densmap of the NM, MMS, and MMU membranes at 250 K. (c) Fluid domain lipid composition of the MMS membrane at 250 K; (d) Voronoi thickness of the MMS membrane at lower temperature ranges; (e) area per lipid <A_L> and membrane thickness <T_L> of different types of lipids (cyclopropane ring containing lipid, fully saturated lipid, monounsaturated lipid, di-unsaturated lipid, and tri-unsaturated lipid) for the three membrane systems at different temperatures. Error bars are calculated over five different trajectory segments of the production run.

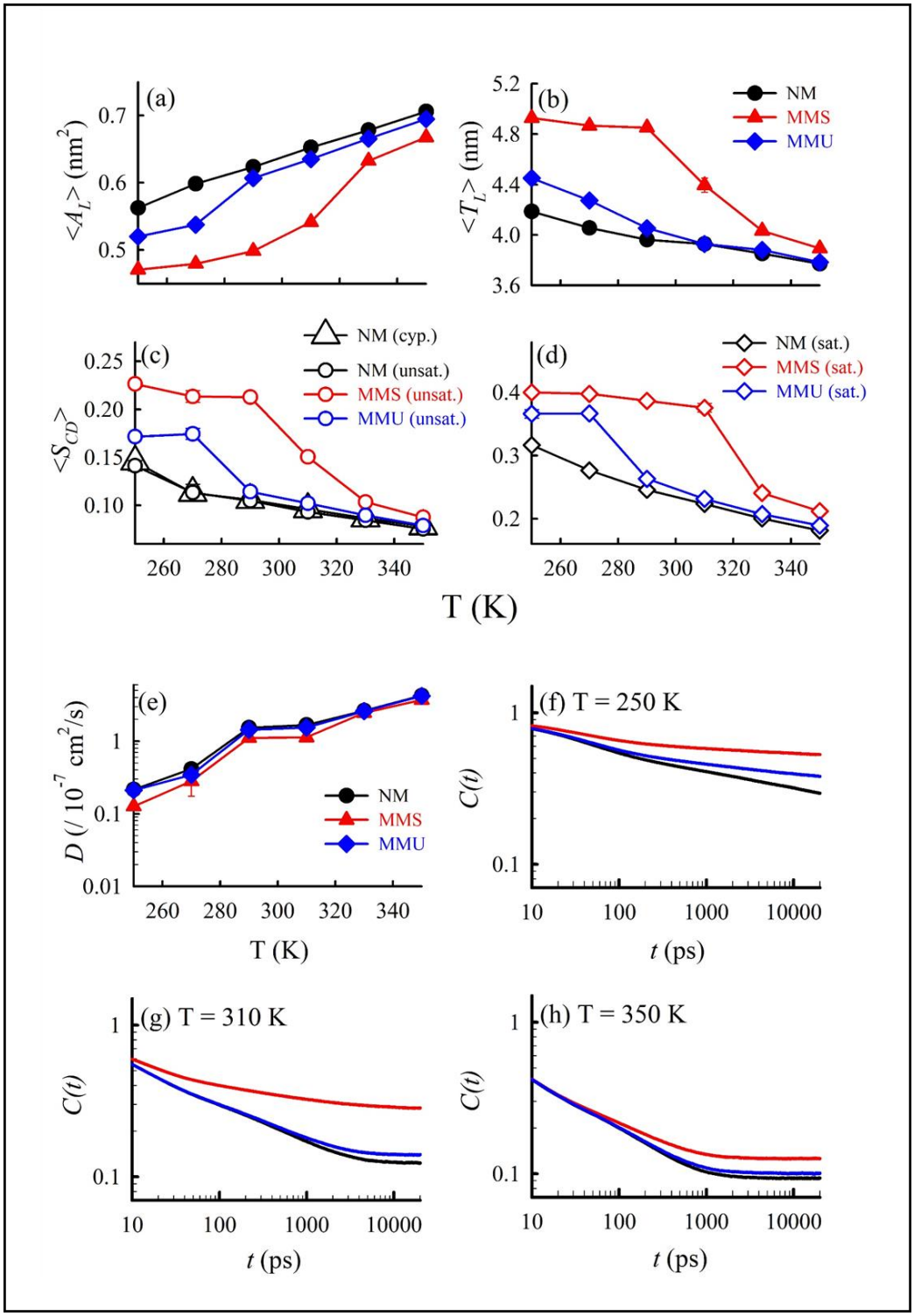

Figure 2: (a) area per lipid, (b) membrane thickness of the entire membrane; (c) and (d) average order parameter $<S_{CD}>$ for different type of acyl chains (based on saturation, unsaturation, and presence of cyclopropane ring); (e) Lateral diffusion coefficient (D_{xy}) of the full membrane as a function of temperature (for NM, MMS, and MMU membrane systems); Rotational decay of the NM, MMS, and MMU membranes at three representative temperatures: (f) 250K, (g) 310K, and (h) 350K. Error bars are calculated over three different trajectory segments of the production run.

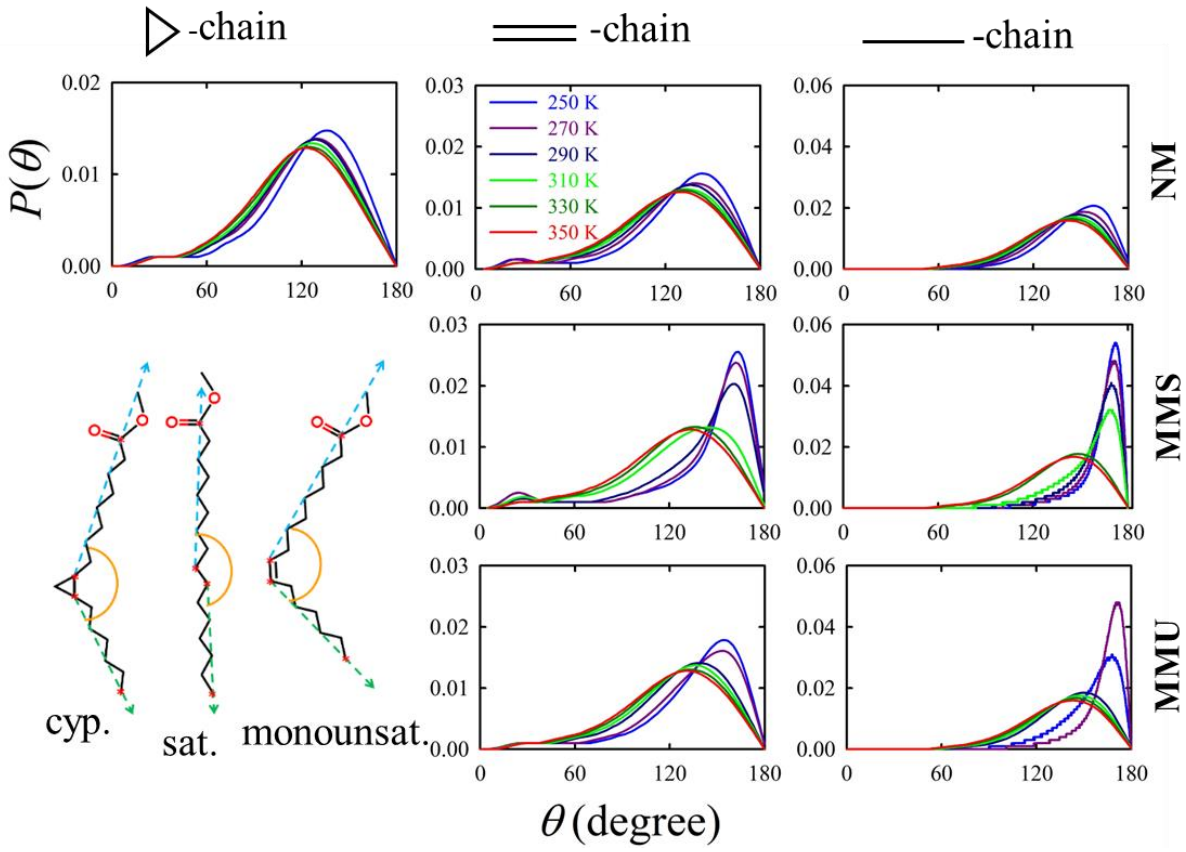

Figure 3: (a) Kink angle distribution of different type of acyl chains (based on saturation, unsaturation and presence of cyclopropane ring) at various temperatures for different membrane systems (NM, MMS, and MMU); (b) schematic diagram of kink angle for different acyl chains.

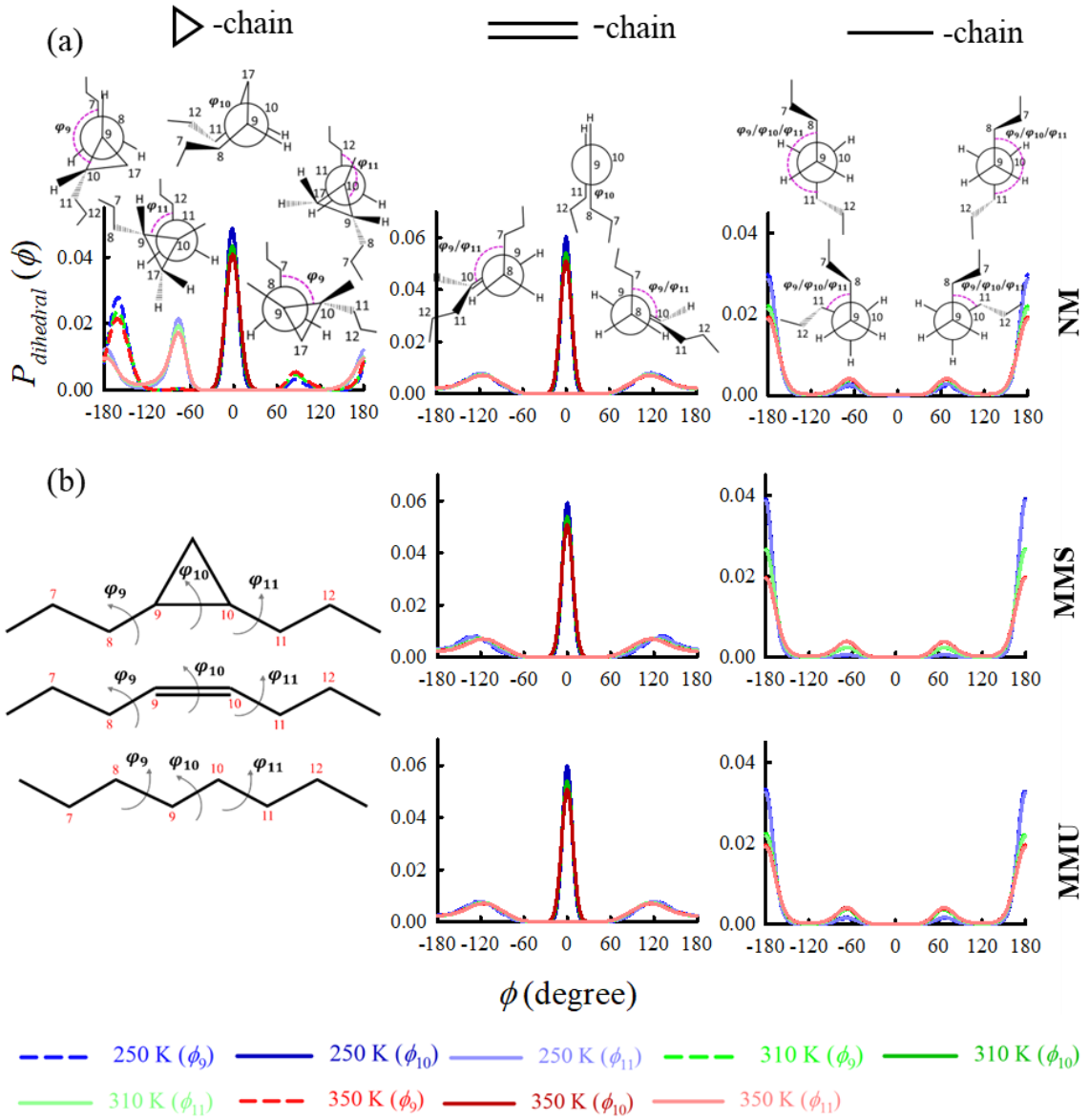

Figure 4: (a) Dihedral angle distribution of the NM membrane system at three representative temperatures: 350, 310, and 250 K. (b) Schematic diagram for distinct type of dihedral angles for different acyl chains.

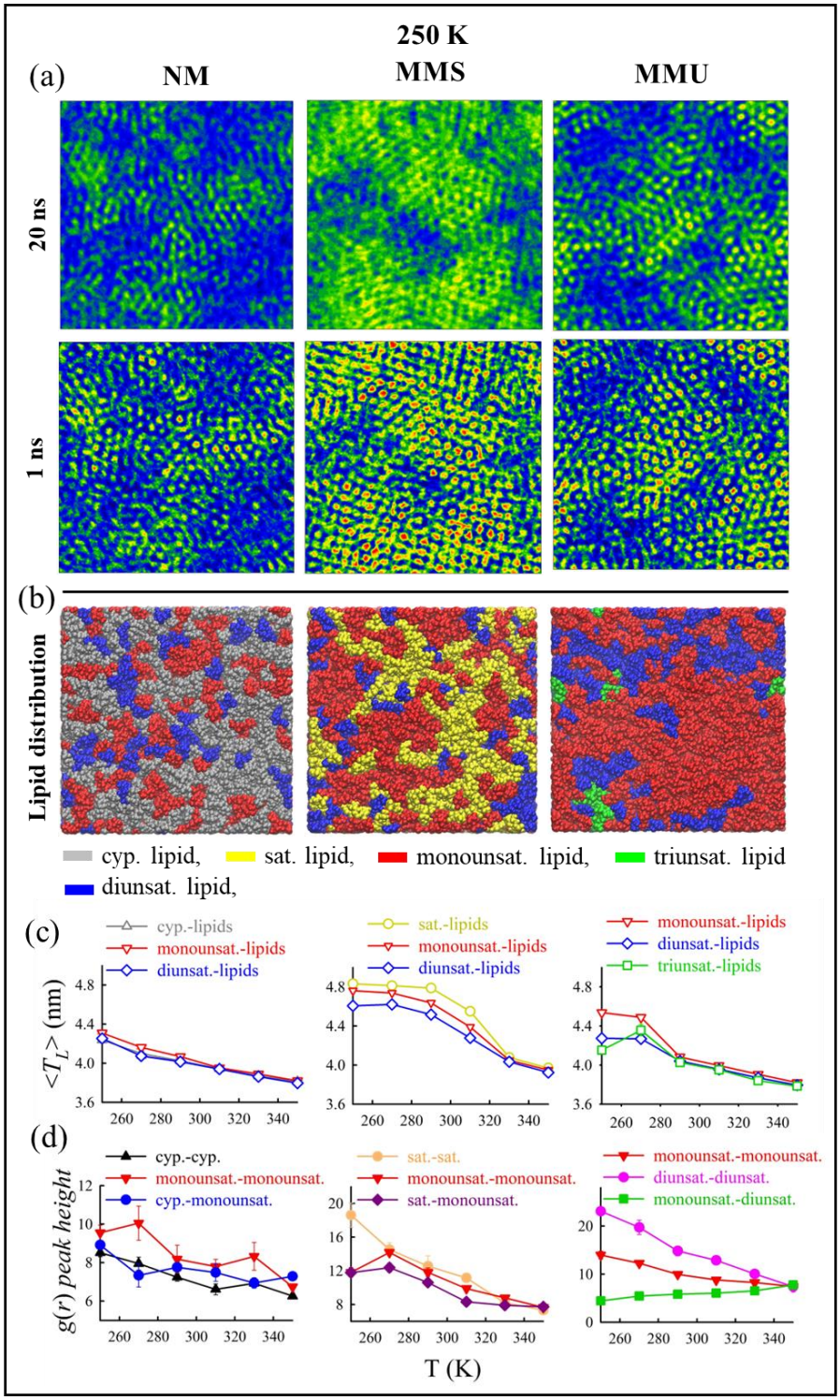

Figure 5. (a) 2D-densmap of the entire membrane at 250 K with respect to two timescales: 20 ns (upper panel) and 1 ns (lower panel); (b) Distribution of different kind of lipids (regarding saturation, unsaturation, and presence of cyclopropane ring) at 250 K; (c) Voronoi analysis-based membrane thickness, (d) peak height of g(r) as a function of temperature for different lipids based on acyl chains (cyclopropane ring containing (cyp.), mono- (monounsat.), di- (diunsat.), tri-unsaturated (triunsat.), and fully saturated (sat.)) of the three membrane systems (NM, MMS, and MMU). Error bars are calculated over three different trajectory segments of the production run.